# The 2022 $M_w$6.2 Pasaman, Indonesia, Earthquake and Its Implication of Seismic Hazard in Central-West Sumatra

**Rizki Wulandari**
National Central University
**Chung-Han Chan** ( hantijun@googlemail.com )
National Central University College of Earth Sciences https://orcid.org/0000-0003-1875-3652
**Adhi Wibowo**
Agency for Meteorology Climatology and Geophysics: Badan Meteorologi Klimatologi dan Geofisika

**Research Article**

**Keywords:** Pasaman Earthquake, Aftershock, b-value, Coulomb Stress Changes, Omori's Law, Earthquake Forecasting, Sumatran Fault, and Sumatra

**Posted Date:** April 14th, 2022

**DOI:** https://doi.org/10.21203/rs.3.rs-1533824/v1

# Abstract

On February 25, 2022, the $M_w$6.2 “Pasaman Earthquake” took place in central-west Sumatra in association with activity in the Sumatran Fault system. This study clarifies the spatial and temporal distribution of the Pasaman Earthquake sequence and forecasts the earthquake sequence’s impact on the seismicity in the vicinity and in the Sumatran Fault system. We first examined the seismicity before the mainshock and observed significant low b-value anomalies both in time and space, shedding light on the earthquake precursor by monitoring b-values prior to the event. Based on the first 18-day aftershocks, we modelled the temporal distribution of the mainshock according to the modified Omori’s law, which suggested this sequence could last 37 or 451 days. To understand the spatial pattern of the aftershocks, we calculated the coseismic Coulomb stress change imparted by the Pasaman Earthquake mainshock. The stress increase extended northwest and southeast, consistent with aftershock distribution. We further evaluated rupture probability for each segment of the Sumatran Fault. Considering the stress perturbation imparted by the Pasaman Earthquake, we expected a seismicity rate increase of ca. 40% at the Sumpur and Sianok segments in the short term. To quantify long-term rupture probability, the recurrence interval and the time elapsed since the previous earthquake were incorporated based on the time-dependent Brownian Passage Time (BPT) model. A high rupture probability is expected for a segment with a short recurrence interval and/or long time elapsed since the last earthquake. The earthquake probability at the Sumani segment in the coming 50 years was determined to be 72.0%. The outcomes of this study are the be-all and end-all for subsequent probabilistic seismic hazard assessment for not only Sumatra, but also certain metropolises in Malaysia and Singapore.


# Introduction

A large, $M_w$6.2 earthquake known as the “Pasaman Earthquake” took place on February 25, 2022 in Pasaman, Indonesia (Figure 1). This earthquake was a shallow earthquake with a hypocentral depth of 12.6 km. Based on the focal mechanism determined by the Agency of Meteorology, Climatology, and Geophysics (BMKG, https://www.bmkg.go.id/en.html), this earthquake was strike-slip faulting (Table 1), which could be associated with activity in the Sumatran Fault system near the Angkola, Barumun, Sumpur, and Sianok segments as shown in Figure 1 (Sieh & Natawidjaja, 2000). In this earthquake sequence, one foreshock of magnitude 5.2 took place four minutes before the mainshock, and 217 aftershocks were recorded until March 15, 2022 (Figure 1). Although this sequence took place in the Sumatran Fault system, these events were in the fault alignment gap between the Angkola and Sianok segments. The occurrence of this sequence makes it urgent to clarify whether the seismicity activity in the fault system will be activated and whether a larger event could take place in the coming future.

Based on the intensity map proposed by BMKG (https://twitter.com/infoBMKG/status/1497028636012351488), the Pasaman Earthquake not only resulted in strong ground motion in the vicinity of the earthquake with a Modified Mercalli Intensity (MMI) value of V, but was also felt as far away as Malaysia and Singapore with a value of II on the MMI scale. The ground shaking in the far field could be attributed to ground motion attenuation behavior (Megawati

et al., 2003) and soft soil amplification (Walling et al., 2012). Based on the characteristics of the path and site effects, the next larger event could result in significant larger ground shaking for the surrounding region, even in the metropolises of Malaysia and Singapore.

Thus, this study aims to clarify the seismicity activity of the Pasaman Earthquake sequence and to forecast the seismicity in this region and the Sumatran Fault system. We first analyzed seismicity activity before the Pasaman mainshock to clarify possible precursory index. We then forecast the spatial and temporal patterns of the aftershock based on coseismic stress change and the modified Omori's law (Utsu, 1961), respectively. To evaluate potential seismic hazard from the Sumatran Fault, we evaluated the rupture probability of each segment by incorporating the active fault parameters and coseismic stress change of the Pasaman Earthquake.

# Seismicity Before The Pasaman Earthquake

To investigate the seismicity in the study region, we accessed the earthquake catalog summarized by BMKG. Most of the seismicity before the Pasaman Earthquake sequence was located on the Angkola and Sianok segments of the Sumatran Fault (Fig. 1), whereas few background events took place near the Pasaman Earthquake mainshock. To understand the evolution of seismic activity in the study region, we modeled the pattern of the frequency-magnitude distribution using the Gutenberg-Richter relation (Gutenberg and Richter, 1954), expressed as:

$$log_{10}N = a - bM$$

,

where $N$ represents the cumulative number of earthquakes with magnitude larger than $M$, and $a$ and $b$ are constants obtained through regression. The b-value is the ratio of small earthquakes to large ones, with a low b-value indicating a higher proportion of large earthquakes. The b-value is usually close to 1.0. Previous studies (e.g., Schorlemmer et al., 2005) indicated that the b-value was related to the stress conditions, that is, a low b-value in a region implies a large differential stress and that this region is toward the end of a seismic cycle. Thus, b-value is an indicator of forthcoming large earthquakes (e.g., Chan et al., 2012).

To clarify whether there was a b-value anomaly before the Pasaman Earthquake, we estimated a temporal variation in b-values for the seismicity within a radius of 40 km of the epicenter. To obtain reliable results, it is crucial to implement a complete portion of the catalog. We thus evaluated magnitude of completeness according to the catalog based on the maximum curvature approach (Wiemer and Wyss, 2000). We evaluated the temporal evolution of b-values 3 years before the mainshock (Fig. 2) and found the b-value in each year to be significantly lower than the ideal b-value of 1.0. Additionally, we found the b-value to drop continuously through the evaluation period and a significantly low b-value of 0.52 in the year preceding the Pasaman Earthquake. This evolution demonstrates a low b-value anomaly both in time and space before the Pasaman Earthquake. It is worth mentioning that the M5.2 foreshock caused

the b-value to decrease, which can be associated as a precursory index of the forthcoming mainshock. The b-value anomaly could indicate stress accumulation in the area and the future occurrence of an earthquake (Main et al., 1989). Based on this concept, monitoring the evolution of b-values evolution could illustrate tectonic stress and forecast the next large earthquakes.

## Spatial And Temporal Distribution Of Aftershocks

Within 18 days after the Pasaman Earthquake mainshock, 217 aftershocks occurred, as reported by BMKG (Fig. 1). The lineation of the aftershock distribution (NW striking) can be associated with the Sumatran Fault system. They fill the gap between the Angkola and Sianok segments.

A large number of aftershocks took place immediately after the mainshock, with the occurrence rate decaying over time. To quantify the aftershock rate evolution, we reported the time interval between each two aftershocks and converted it into a daily interval rate (Fig. 3). This showed a significantly higher rate than the background interval rate before this sequence and that the daily interval rate is more than 10 times higher than the background rate even 18 days after the mainshock (the end of the available catalog). Using the modified Omori's law (Utsu, 1961), we modeled the seismicity rate evolution, expressed as:

$$n(t) = \frac{K}{(C + t)^P}$$

,

where *n(t)* represents the seismicity rate as a function of time *t* since the mainshock, *K* represents the amplitude of the rate, *C* represents the time delay of rate decay, and *P* represents the decay rate. Through regression, we obtained best fits of *K*, *P*, and *C*, which resulted in the rate evolution of the aftershocks being expressed as:

$$n = \frac{40}{(0.3 + t)^{1.8}}$$

.

Considering the daily seismicity rate before this sequence (0.057 events per day), this aftershock sequence could last 37 or 451 days, considering the average and deviation of the Omori decay, respectively.

## Coseismic Stress Evolution Associated With Subsequent Aftershocks

Rupture on a fault plane causes deformation in the vicinity, which can be converted into Coulomb stress change (ΔCFS) on a specific focal mechanism. Previous studies (e.g., King et al., 1994) concluded that

an increase in Coulomb stress could trigger aftershocks or even a subsequent larger earthquake. The ΔCFS can be expressed as (Harris, 1998):

$$\Delta CFS = \Delta\tau + \mu_s'\Delta\sigma_e$$

,

where $\Delta CFS$ is the amount of change in Coulomb stress, $\Delta\tau$ is shear stress, $\Delta\sigma_e$ is the normal stress, and $\mu_s'$ is the effective friction coefficient, usually assumed to be 0.4. To estimate the change in Coulomb stress, an elastic half-space model on an assumed isotropic-homogenous rectangular plane is used (Okada, 1992). The ΔCFS calculation in this study is based on the COULOMB 3.3 program (Toda, 2005).

Since a detailed slip dislocation model for the Pasaman Earthquake is unavailable, we proposed a slip model (Table 1) based on the earthquake parameters and scaling law (Wells & Coppersmith, 1994 ) for ΔCFS calculation. Since the focal mechanisms of the aftershocks are unavailable, we assumed the faulting type in this region is consistent with the focal mechanism of the mainshock (Table 1). To calculate ΔCFS, we followed the procedure proposed by Catalli & Chan (2012) to obtain the maximum ΔCFS at different depths among the seismogenic layer (the depth between 0 and 20 km) to minimize calculation uncertainty, especially in the vicinity of the coseismic rupture patch.

Using the above procedure, the Coulomb stress changes imparted by the Pasaman Earthquake to the surrounding right-lateral strike-slip fault (with μ’=0.4) were obtained (shown in Fig. 4). The stress increase extended northwest and southeast of the coseismic slip alignment (the green line in Fig. 4), consistent with the aftershock pattern (yellow circles in Fig. 4).

## Seismic Hazard From The Sumatran Fault System

An increase in Coulomb stress could not only trigger aftershocks but also enhance the probability of the next larger earthquake. The Pasaman Earthquake took place in the Sumatran Fault system, where there was a potential for devastating earthquakes (Sieh and Natawidjaja, 2000). To evaluate the seismic hazard of the Pasaman Earthquake, we considered the ΔCFS imparted by the Pasaman Earthquake and the fault parameters of the Sumatran Fault.

A map view of the ΔCFS (Fig. 4) illustrates a general pattern of stress change on the Sumatran Fault. According to this map view, stress in the Sumpur, Sianok, Sumani, and Angkola segments was promoted while stress in the Barumun segment was dropped. To specify the stress change in these segments, their mechanisms (Table 2) and alignments were implemented in the ΔCFS calculation (Fig. 5). The stresses in the Sumpur and Sianok segments were significantly enhanced, with a maximum ΔCFS of 0.1 bar, and the stresses in the Sumani and Angkola segments were slightly enhanced, with a maximum ΔCFS of 0.03 and 0.01 bars, respectively. To quantify the impact of the seismicity rate based on ΔCFS, we

implemented the rate-and-state friction model (Dieterich, 1994). This model evaluates seismicity rate evolution $\Delta R(t)$ using ΔCFS and is expressed as:

$$\Delta R(t) = \frac{\lambda}{[exp(-\frac{\Delta CFS}{A\sigma}) - 1]exp(-\frac{t-t_n}{t_{na}}) + 1}$$

,

where $\lambda$ represents long-term seismicity rate; $A\sigma$ represents a constitutive parameter of the model, assumed to be 0.3 (Chan et al., 2017); $t_n$ represents the occurrence time of the earthquake that caused the ΔCFS; and $t_{na}$ represents aftershock duration, obtained from our Omori's model (Fig. 3).

Based on the rate-and-state friction model and stress change, the rate perturbation by the Pasaman Earthquake could be evaluated at each segment of the Sumatran Fault (Table 2). Due to a significant stress increase in the Sumpur and Sianok segments, we expected a seismicity rate increase of ca. 40%. The seismicity rates in the Sumani and Angkola could rise by 10.5% and 3.4%, respectively, whereas the Barumum segment could be farther from the next earthquake due to coseismic stress drop.

The short-term rate perturbation imparted by the Pasaman event has been evaluated for the Sumatran fault. To quantify its long-term rupture probability, we considered the recurrence interval of each fault segment (Table 2). The rupture probability could be quantified using a Poisson process, which is widely applied for probabilistic seismic hazard assessment (Cornell, 1968), expressed as follows:

$$P = 1 - e^{-\nu \bullet t}$$

,

where $P$ represents the rupture probability of a fault, $\nu$ represents the annual seismicity rate of the fault segment, and t represents the time period of interest.

Using this model, each segment's rupture probability in the coming 50 years could be quantified (Table 2). A high rupture probability of ca. 60% was obtained for the Sumpur segment due to its short recurrence interval (55 years). Generally, the earthquake probabilities on all these segments are rather high, due to their high slip rates (14 mm/year).

In addition to the stationary probability based on the assumption of the Poisson process mentioned above, for segments where data from at least one previous earthquake were recorded, evaluation of rupture probability can be further improved by including the record of the previous earthquake(s). The time elapsed since the previous event could be incorporated into the time-dependent Brownian Passage Time (BPT) model (Ellsworth et al., 1999). The BPT model has been applied to many probabilistic seismic hazard assessments (e.g., Fujiwara, 2014), and its credibility has been confirmed by comparing it to paleo-seismic data (Gao et al., 2022). The density function (DF) of this model can be expressed as:

$$DF = \left( \frac{\mu}{2\pi\alpha^2 t^3} \right)^{1/2} \exp\left( - \frac{(t-\mu)^2}{2\alpha^2 \mu t} \right)$$

,

where $\mu$ represents the mean recurrence interval, $t$ represents the time elapsed since last earthquake, and $\alpha$ represents the aperiodicity, whose value is usually between 0.3 and 0.7 and is assumed to be 0.5 (Chan et al., 2019). Based on this model, the rupture probabilities for the Angkola, Sianok, and Sumani segments (with records of previous events) were evaluated (shown in Fig. 6). A high rupture probability is expected for a segment with a short recurrence interval and/or long time elapsed since the last earthquake. The earthquake probability at the Sumani segment in the coming 50 years could be 72.0%. Based on the BPT model, these three segments obtained higher rupture probabilities compared to the probabilities obtained via the time-dependent Poisson process, which can be attributed to a long time elapsed since the last earthquake.

# Conclusions

This study clarifies the seismicity activity of the Pasaman Earthquake sequence and aims to forecast the seismicity in this region and the Sumatran Fault system. Based on the seismicity before the mainshock, a significantly low b-value anomaly was observed. This analysis shed light on the earthquake's precursor via analysis of the evaluation of the b-values prior to the earthquake. We also discussed the spatial and temporal distribution of the aftershocks and modeled them through the coseismic Coulomb stress change imparted by the Pasaman Earthquake mainshock and the modified Omori's law, respectively. The outcome could help us understand the pattern of forthcoming aftershocks, including aftershock duration. To evaluate potential seismic hazard from the Sumatran Fault, fault parameters and coseismic stress of the Pasaman Earthquake were implemented to evaluate the rupture probability of each segment. The result suggests the rupture probability of each segment is very high. The $M_w$6.2 Pasaman Earthquake rattled Malaysia and Singapore; the next larger events taking place along the Sumatran Fault could result in significantly stronger ground motion and threaten not only Sumatra, but also some metropolises in the far-field.

# Declarations

### Declaration of Competing Interest

The authors declare that they have no known competing financial interests or personal relationships that could have appeared to influence the work reported in this paper.

### Availability of data and materials

The datasets implemented in study is available from the corresponding author upon reasonable request.

**Acknowledgments**

We thank Shinji Toda and Ross S. Stein for providing Coulomb 3.3. This study was supported by the Ministry of Science and Technology in Taiwan—under grants MOST 109-2116-M-008-029 -MY3, MOST 110-2124-M-002-008, and MOST 110-2634-F-008-008. This work is financially supported by the Earthquake Disaster & Risk Evaluation and Management Center (E-DREaM) from the Featured Areas Research Center Program within the framework of the Higher Education Sprout Project by the Ministry of Education in Taiwan. The authors also thank the Agency of Meteorology, Climatology and Geophysics (BMKG) for providing the data.

# References

1. Catalli, F., & Chan, C. H. (2012). New insights into the application of the Coulomb model in real-time. *Geophysical Journal International*, *188*(2), 583–599. https://doi.org/10.1111/j.1365-246X.2011.05276.x
2. Chan, C., Ma, K., Lee, Y., & Wang, Y. (2018). Rethinking Seismic Source Model of Probabilistic Hazard Assessment in Taiwan after the 2018 Hualien, Taiwan, Earthquake Sequence. *Seismological Research Letters*, *90*(1), 88–96. https://doi.org/10.1785/0220180225
3. Chan, C., Wang, Y., Wang, Y., & Lee, Y. (2017). Seismic-Hazard Assessment over Time: Modeling Earthquakes in Taiwan. *Bulletin of the Seismological Society of America*, *107*(5), 2342–2352. https://doi.org/10.1785/0120160278
4. Cornell, C. A. (1968). Engineering seismic risk analysis. *Bulletin of the Seismological Society of America*, *58*(5), 1583–1606. https://doi.org/10.1785/BSSA0580051583
5. Dieterich, J. (1994). A constitutive law for rate of earthquake production and its application to earthquake clustering. *Journal of Geophysical Research: Solid Earth*, *99*(B2), 2601–2618. https://doi.org/https://doi.org/10.1029/93JB02581
6. Ellsworth, W. L., Matthews, M. V, Nadeau, R. M., Nishenko, S. P., Reasenberg, P. A., & Simpson, R. W. (1999). *A physically-based earthquake recurrence model for estimation of long-term earthquake probabilities*.
7. Fujiwara, H. (2014). *Seismic Hazard Maps for Japan* (pp. 1–28). https://doi.org/10.1007/978-3-642-27737-5_617-1
8. Gao, J., Tseng, Y., and Chan, C. (2022). Validation of the probabilistic seismic hazard assessment by the Taiwan Earthquake Model through comparison with strong ground motion observations, *accepted by Seismological Research Letters*.
9. Gutenberg, B., & Richter, C. F. (1944). Frequency of earthquakes in California*. *Bulletin of the Seismological Society of America*, *34*(4), 185–188. https://doi.org/10.1785/BSSA0340040185
10. Harris, R. A., & Simpson, R. W. (1998). Suppression of large earthquakes by stress shadows: A comparison of Coulomb and rate-and-state failure. *Journal of Geophysical Research: Solid Earth*, *103*(10), 24439–24451. https://doi.org/10.1029/98jb00793

11. Irsyam, M., Cummins, P. R., Asrurifak, M., Faizal, L., Natawidjaja, D. H., Widiyantoro, S., Meilano, I., Triyoso, W., Rudiyanto, A., Hidayati, S., Ridwan, M., Hanifa, N. R., & Syahbana, A. J. (2020). Development of the 2017 national seismic hazard maps of Indonesia. *Earthquake Spectra*, *36*(1_suppl), 112–136. https://doi.org/10.1177/8755293020951206
12. King, G. C. P., Stein, R. S., & Jian Lin. (1994). Static stress changes and the triggering of earthquakes. *Bulletin - Seismological Society of America*, *84*(3), 935–953. https://doi.org/10.1016/0148-9062(95)94484-2
13. Main, I. G., Meredith, P. G., & Jones, C. (1989). A reinterpretation of the precursory seismic b-value anomaly from fracture mechanics. *Geophysical Journal International*, *96*(1), 131–138. https://doi.org/10.1111/j.1365-246X.1989.tb05255.x
14. Megawati, K., Pan, T. C., & Koketsu, K. (2003). Response spectral attenuation relationships for Singapore and the Malay Peninsula due to distant Sumatran-fault earthquakes. Earthquake engineering & structural dynamics, 32(14), 2241–2265.
15. Okada, Y. (1992). Internal deformation due to shear and tensile faults in a half-space. *Bulletin - Seismological Society of America*, *82*(2), 1018–1040.
16. Schorlemmer, D., Wiemer, S., & Wyss, M. (2005). Variations in earthquake-size distribution across different stress regimes. *Nature*, *437*(7058), 539–542. https://doi.org/10.1038/nature04094
17. Sieh, K., & Natawidjaja, D. (2000). Neotectonics of the Sumatran fault, Indonesia. *J. Geophys. Res.*, *105*, 28 295 – 28 326.
18. Toda, S. (2005). Coulomb 3.3 Graphic-rich deformation and stress-change software for earthquake, tectonic, and volcano research and teachin. *USGS Open-File Report*, 63. http://www.coulombstress.org/download
19. Utsu, T. (1961). A statistical study on the occurrence of aftershocks. *Geophysical Magazine*, *30*, 521–605.
20. Walling, M. Y., Megawati, K., & Zhu, C. (2012). Estimation of Vs30 Soil Profile Structure of Singapore from Microtremor Records. *EGU General Assembly Conference Abstracts*, 6757.
21. Wells, D. L., & Coppersmith, K. J. (1994). New empirical relationships among magnitude, rupture length, rupture width, rupture area, and surface displacement. *Bulletin - Seismological Society of America*, *84*(4), 974–1002.
22. Wiemer, S., & Wyss, M. (2000). Minimum magnitude of completeness in earthquake catalogs: Examples from Alaska, the Western United States, and Japan. *Bulletin of the Seismological Society of America*, *90*(4), 859–869. https://doi.org/10.1785/0119990114

# Tables

**Table 1.** The source parameters of the Pasaman Earthquake

| Date (yyyy/mm/dd) | Lat (°N) | Long (°E) | Depth (km) | $M_w$ | Strike (°) | Dip (°) | Rake (°) | Length (km)* | Width (km)* |
|---|---|---|---|---|---|---|---|---|---|
| 2022/02/25 | 0.15 | 99.98 | 12.6 | 6.2 | 133 | 76 | 175 | 17.99 | 8.45 |

*The length and the width were estimated based on the empirical relations of Wells & Coppersmith, 1994.

**Table 2.** The fault parameters for the segment of the Sumatran Fault in the vicinity of the Pasaman Earthquake (Irsyam et al., 2020). The records for historical earthquakes were obtained by Sieh & Natawidjaja, 2000. The probability of rupture in the next 50 years for each segment is evaluated using the Poisson process and the BPT model for segments where at least one earthquake was recorded.

| ID | Segment | Last earthquakes | Time elapse (until 2022) | Expected magnitude | Slip Rate (mm/yr) | Recurrence Interval (years) | Max ΔCFS (bars) | Short-term rate change | Rupture probability in 50 years |
|---|---|---|---|---|---|---|---|---|---|
| 1 | Angkola | 1892 | 130 | 7.7 | 14 | 291 | 0.01 | 3.4% | 15.8%, 16.5% |
| 2 | Barumun | No record | N/A | 7.5 | 14 | 192 | -0.01 | -3.3% | 22.9%, NA |
| 3 | Sumpur | No record | N/A | 6.9 | 14 | 55 | 0.10 | 39.6% | 59.7%, NA |
| 4 | Sianok | 1926 | 96 | 7.4 | 14 | 156 | 0.10 | 39.6% | 27.4%, 41.2% |
| 5 | Sumani | 1943 | 79 | 7.1 | 14 | 84 | 0.03 | 10.5% | 44.9%, 72.0% |

# Figures

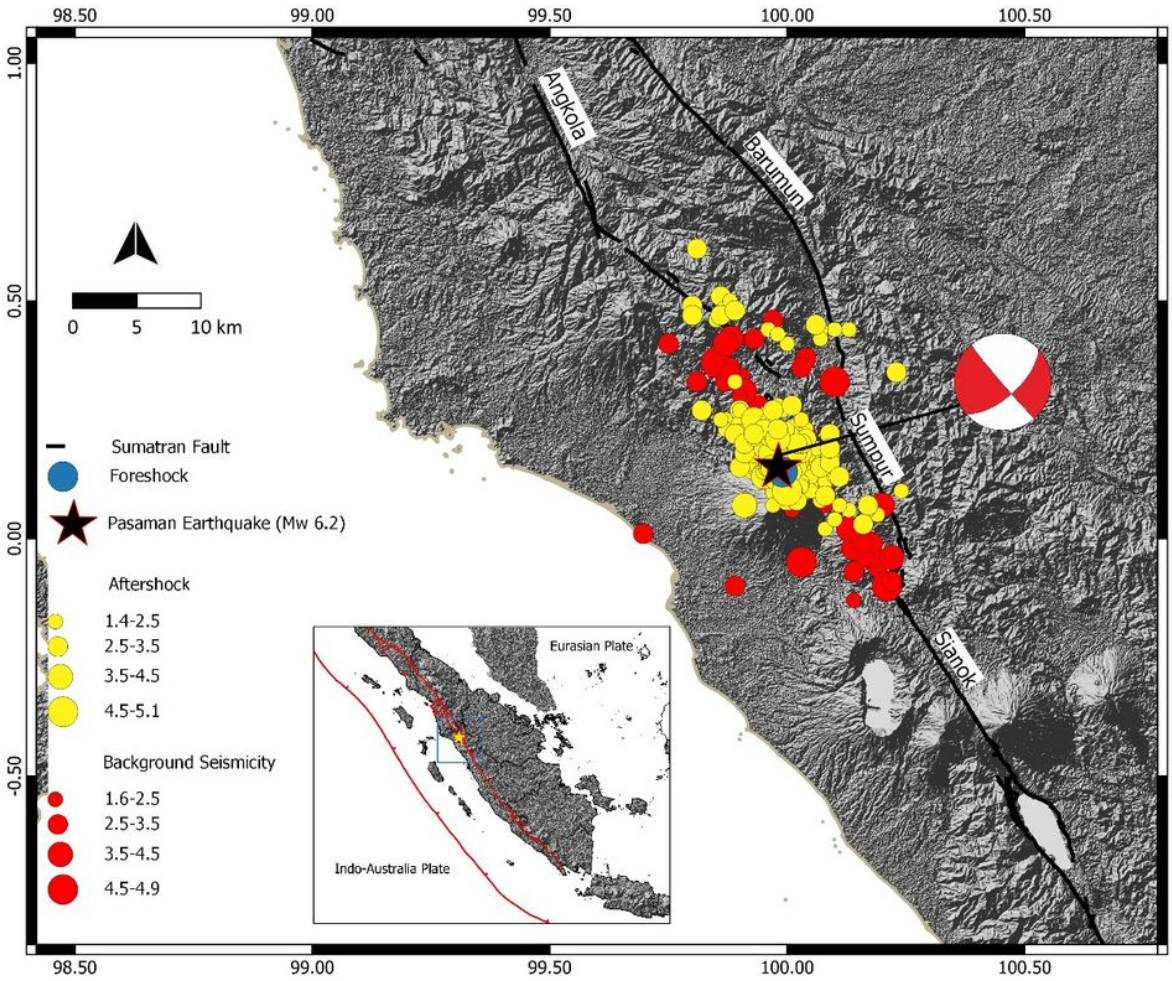


## Figure 1

Distribution of seismicity before (red circles) and after (yellow circles) the Pasaman Earthquake (star). The foreshock is shown with the blue circle. The focal mechanism was determined by BMKG. The black lines denote segments of the Sumatran fault (Sieh & Natawidjaja, 2000).

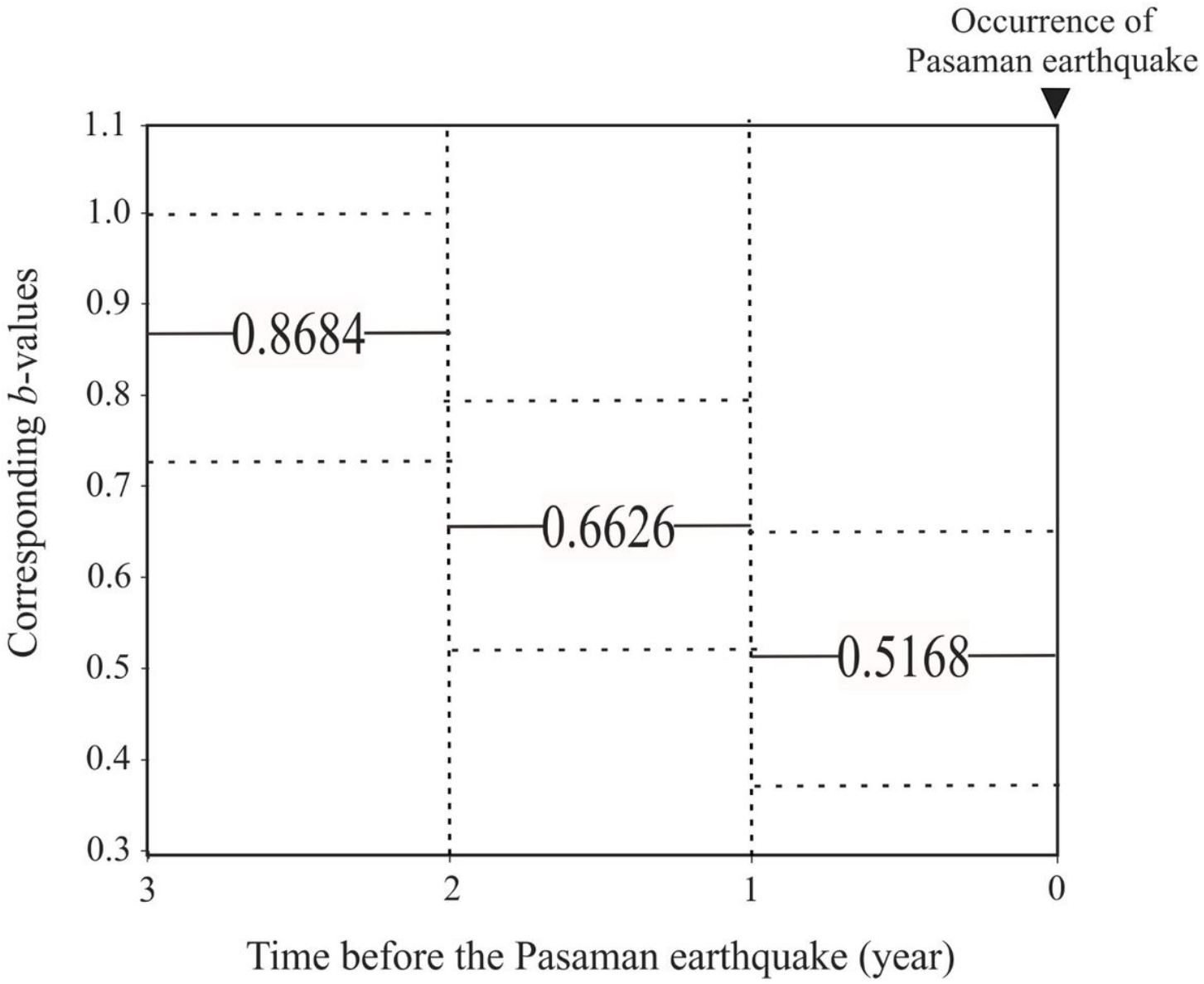


## Figure 2

Average of b-values (solid lines) and standard deviations (dashed lines). We considered the earthquakes within 40 km of the Pasaman Earthquake.

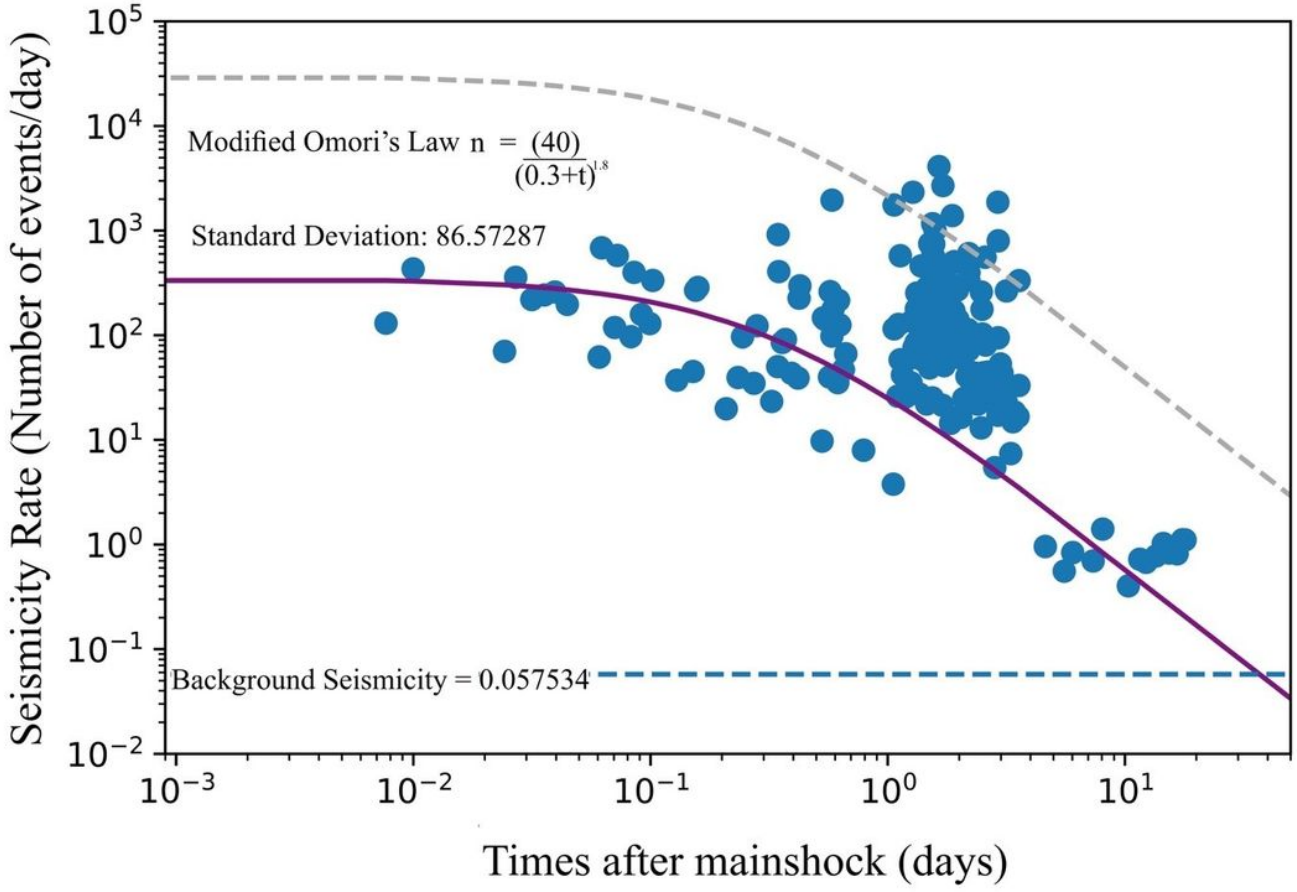


## Figure 3

Observed (blue circles) and modelled (purple line) temporal distribution of the Pasaman Earthquake aftershocks. The modeled distribution was obtained using the modified Omori's law (Utsu, 1961) through regression of the observations. The standard deviation of the regression is shown in dashed grey lines. The background seismicity rate is shown as a dashed blue line.

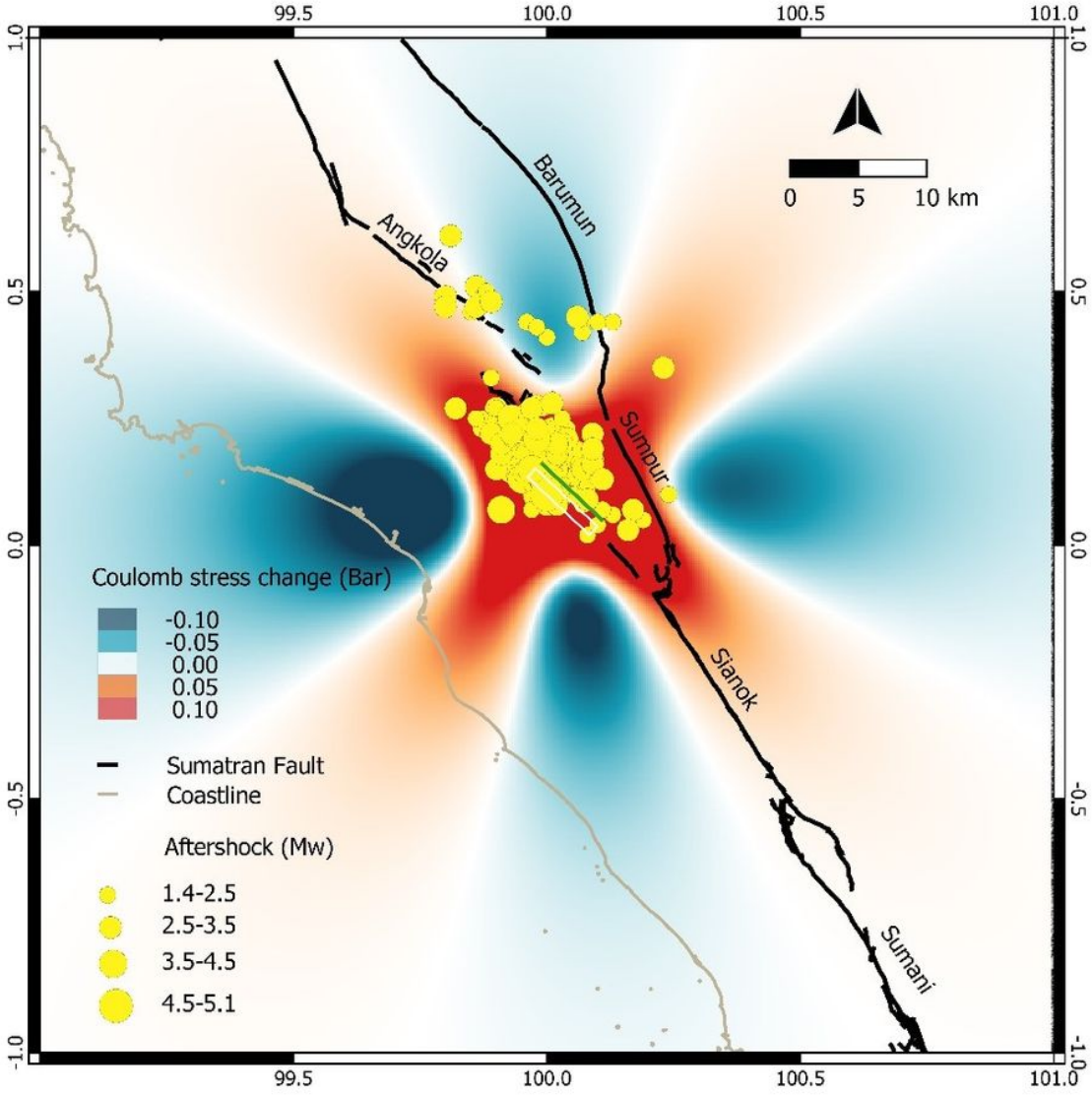


## Figure 4

Distribution of aftershocks (yellow circles) and Coulomb stress changes associated with the $M_w$6.2 Pasaman Earthquake. The rupture parameter of the mainshock is shown in Table 1. The green line is the rupture zone of the Pasaman Earthquake. The specified receiver fault is assumed to be the same as the focal mechanism of the mainshock (Table 1).

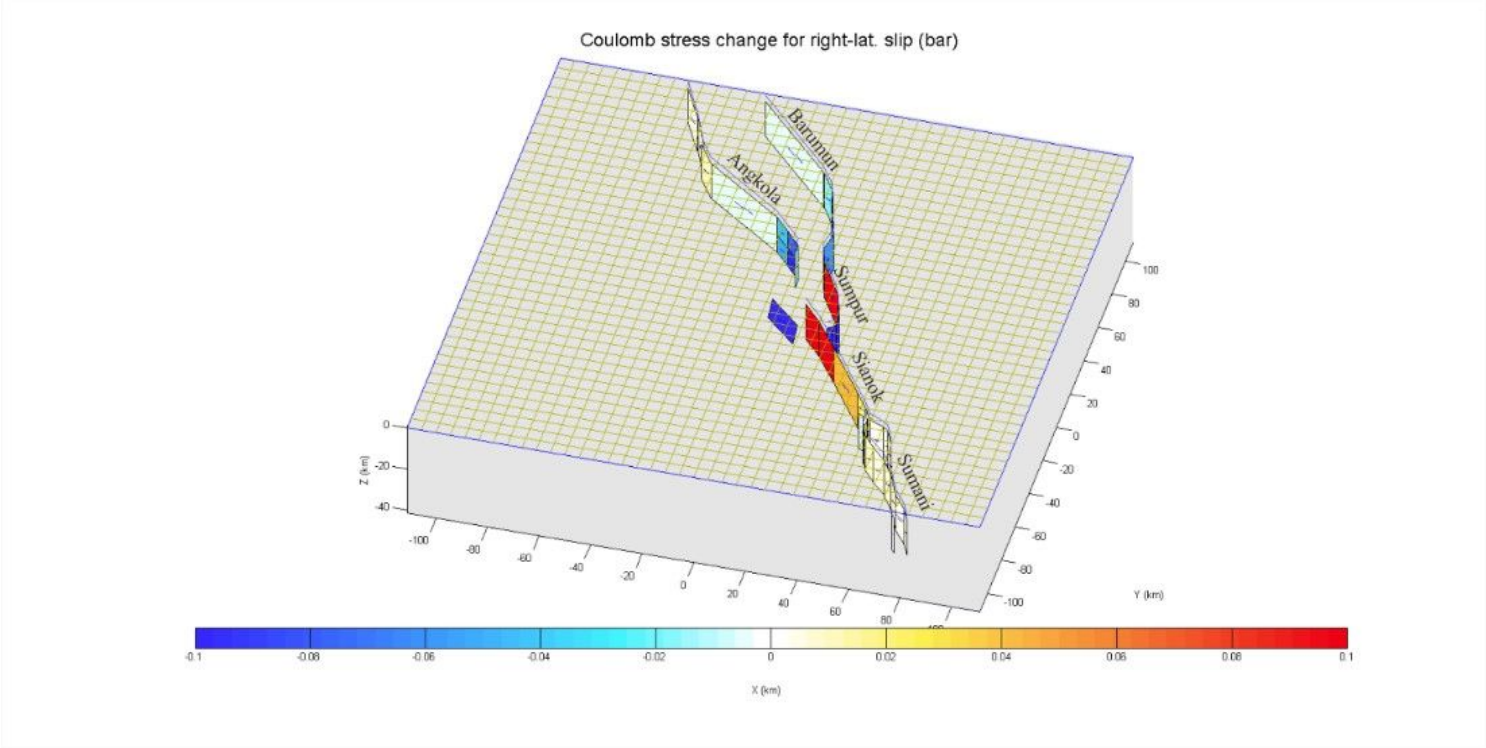


## Figure 5

Coulomb stress changes at each segment of the Sumatran Fault. The maximum ΔCFS on each segment was reported in Table 2.

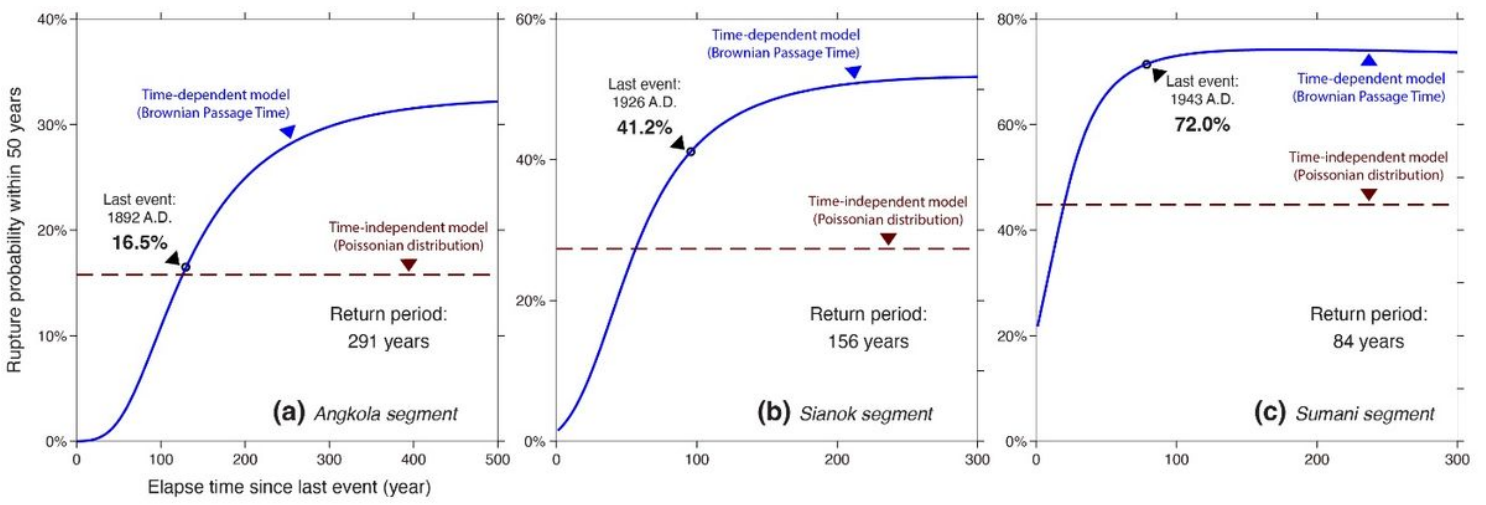


## Figure 6

Rupture probabilities in the coming 50 years for (a) Angkola, (b) Sianok, and (c) Sumani segments considering the BPT model (blue solid lines) and Poisson distribution (red dashed lines).